

Seasonal light absorption properties of water-soluble brown carbon in atmospheric fine particles in Nanjing, China



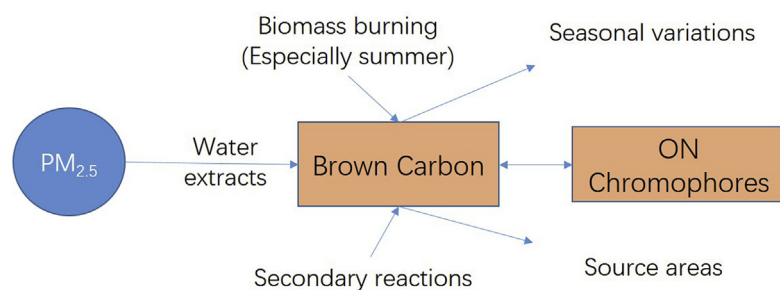
Yanfang Chen^a, Xinlei Ge^{a,*}, Hui Chen^a, Xinchun Xie^a, Yuntao Chen^a, Junfeng Wang^a, Zhaolian Ye^b, Mengying Bao^c, Yanlin Zhang^c, Mindong Chen^a

^a Jiangsu Key Laboratory of Atmospheric Environment Monitoring and Pollution Control (AEMPC), Collaborative Innovation Center of Atmospheric Environment and Equipment Technology (CIC-AEET), School of Environmental Science and Engineering, Nanjing University of Information Science and Technology, Nanjing 210044, China

^b College of Chemistry and Environmental Engineering, Jiangsu University of Technology, Changzhou 213001, China

^c Yale-NUIST Center on Atmospheric Environment, Nanjing University of Information Science and Technology, Nanjing 210044, China

GRAPHICAL ABSTRACT



ARTICLE INFO

Keywords:

Brown carbon
Light absorption
Aerosol mass spectrometry
Secondary aerosol
Biomass burning

ABSTRACT

Recently atmospheric brown carbon (BrC) is recognized as an important contributor to light absorption and positive climate forcing. In this work, daily fine particulate matter (PM_{2.5}) samples were collected over a full year (May 2015–May 2016) in Nanjing, and seasonal light absorption properties of water-soluble BrC were investigated. We found that winter samples had the strongest light absorption among four seasons. The light absorption at 365 nm (Abs_{365}) for all seasons linked closely with secondary organic carbon (SOC), indicating a dominant contribution from secondary sources to BrC. However primary biomass burning might also contribute to BrC as revealed by the good correlations of Abs_{365} versus levoglucosan fragments and/or K^+ , and such influence was more evident during summer. Furthermore, an Aerodyne soot-particle aerosol mass spectrometer (SP-AMS) was employed to determine the elemental ratios of BrC. We found that except in winter, the Abs_{365} in general positively correlated with the average oxidation states (OS_c) of BrC, suggesting more BrC were produced at higher OS_c . The mass absorption efficiency at 365 nm (MAE_{365}) showed no clear dependences on OS_c during spring, summer and fall, but decreased against OS_c during winter, indicating chemical aging may lead to photo-bleaching of BrC in winter. Moreover, positive responses of Abs_{365} and MAE_{365} to N/C ratios were found during all seasons, indicating nitrogen-containing organics can be important BrC chromophores. Potential source areas of BrC were further discussed to improve our understanding of BrC sources in this region.

* Corresponding author.

E-mail address: caxinra@163.com (X. Ge).

1. Introduction

Atmospheric aerosol particles play an important role in earth's radiation budget and global climate change (e.g., Carlsaw et al., 2010). Black carbon (BC) is typically treated as the most important aerosol component leading to positive radiative forcing (e.g., Bond et al., 2013; Wang et al., 2017). While recent studies indicate that a certain fraction of organic aerosols, often called “Brown carbon (BrC)” can also absorb lights at the wavelengths of near-ultraviolet (UV) and visible ranges (e.g., Bahadur et al., 2012; Cappa et al., 2012; Chen and Bond, 2010; Kirchstetter et al., 2004; Lack et al., 2012a; Laskin et al., 2015; Pokhrel et al., 2017; Saleh et al., 2013; Saleh et al., 2014). The radiative forcing of BrC has been estimated to be 19–24% of the total aerosol absorption (Feng et al., 2013; Liu et al., 2015; Zhang et al., 2017a).

Both laboratory and field studies have shown that BrC can be produced from multiple sources, including primary emissions from fossil fuel combustion (Bond et al., 2002; Yan et al., 2017) and biomass burning (Chakrabarty et al., 2010; Lack et al., 2012a; Washenfelder et al., 2015), as well as secondary formation through various reaction pathways including gas-phase and aqueous reactions (e.g., Hems and Abbatt, 2018; Laskin et al., 2015; Lin et al., 2015; Saleh et al., 2013; Zhong and Jang, 2011). The absorptivities of BrC generated from different sources are highly variable due to the different structures and concentrations of BrC chromophores (Laskin et al., 2015; Nguyen et al., 2012; Xie et al., 2017). A number of studies have been conducted to identify the BrC chromophores, but only a small fraction of organic chromophores have been identified, including nitrophenols, aromatic carbonyls, oxygenated–conjugated compounds, nitroaromatics and sulfur-containing compounds (e.g., Desyaterik et al., 2013; Lin et al., 2015; Teich et al., 2017; Xie et al., 2017).

The BrC absorption can be directly measured by filter-based online instruments (Kirillova et al., 2016; Nakayama et al., 2015), such as the multi-angle absorption photometer (MAAP) and non-filter-based instruments (Laskin et al., 2015; Shamjad et al., 2015), such as photoacoustic spectroscopy (PAS) and cavity ring-down (CRD) spectroscopy (Lack et al., 2006, 2012a, 2012b; Pokhrel et al., 2016, 2017). Moreover, water-soluble BrC has been measured semi-continuously by a particle-into-liquid sampler (PILS), coupled to a liquid waveguide capillary cell (LWCC) and an absorbance spectrometer (Liu et al., 2013; Satish et al., 2017). In addition, offline light absorption measurements on filter extracts have been conducted in both laboratory (e.g., Chen and Bond, 2010; Liu et al., 2016) and field studies (e.g., Chen et al., 2016; Zhang et al., 2017c). The advantage of this approach is that the interference by BC can be avoided. Compared to the online methods, offline technique can be easily performed in combination with other offline measurements for a better characterization of BrC.

The Yangtze River Delta (YRD) region is one of the most populated areas in China. Nanjing, as the second largest city and the provincial capital of Jiangsu Province, is also facing severe air pollution issue (Wang et al., 2016a). Some studies (e.g., Wu et al., 2017; Zhang et al., 2017b; Zhang et al., 2015) show that the organic aerosols (OA) can account for a remarkable proportion of fine aerosol mass and are originated from multiple sources, including primary (traffic, cooking, industry, biomass burning and biogenic emissions, etc.) and secondary sources (aqueous-phase and photochemical processing). Hundreds of organic species (polycyclic aromatic hydrocarbons, carboxylic/dicarboxylic acids, hopanes, phthalates, amines and amino acids, etc.) have been identified (e.g., Wang et al., 2011; Wang et al., 2009; Wang et al., 2007). Recently, a 3-year result of light absorption of BrC in Nanjing based on continuous measurement combined with Mie-theory calculations was reported (Wang et al., 2018). The results demonstrate a significant contribution of BrC to total aerosol absorption (from 6% to 18%, and up to ~28% in biomass burning dominant season and winter). Nevertheless, studies regarding the light absorption of BrC are still scarce in this region. In this work, we investigated the light absorption properties of the water-soluble BrC via a series of offline

measurements for PM_{2.5} samples collected in Nanjing during 2015–2016. We focus on its seasonal behaviors, sources and dependences on bulk chemical properties.

2. Experimental methods

2.1. Sample collection

A high-volume sampler (Laoying Ltd., Qingdao, model 2031) with a flow rate of 1.05 m³ min⁻¹ was set on rooftop of a seven-floor building (~21 m above the ground) inside the campus of Nanjing University of Information Science and Technology in the northern suburb of Nanjing (32.21°N, 118.72°E) (Fig. S1 in the supplement). More details can be found in our previous study (Wang et al., 2016b). A total of 272 PM_{2.5} samples were collected daily (22 h, from 12:00 p.m. to 10:00 a.m. of the next day) from May 4, 2015 to 4 May 2016. The samples were collected onto pre-baked (450 °C for 4 h) quartz fiber filters (8 × 10 inch, Pall Life Science, USA). Two field blanks were treated in the same manner as for the samples. The PM_{2.5} mass concentrations were determined gravimetrically using a digital balance (OHAUS DV215CD, precision 0.01 mg) immediately after filter collection. The filters were then wrapped in aluminum foil, sealed in polyethylene bags and stored at -18 °C until analysis.

During sampling, meteorological parameters (temperature, relative humidity, wind speed, wind direction) were recorded at the meteorological station located near the sampling site (~50 m distance). Original hourly data were averaged into daily data.

2.2. Chemical analyses

OC/EC: One punched piece (diameter: 17 mm) of each filter was analyzed for organic carbon (OC) and elemental carbon (EC) contents by the thermal-optical OC/EC analyzer (Sunset Laboratory, USA) following the standard protocol (Birch and Cary, 1996; Cao et al., 2017).

Ionic species: Two 10 mm diameter filter punches of each filter were extracted with 15 mL ultrapure water (18.2 MΩ cm, TOC < 5 ppb), sonicated for 40 min at 0 °C in an ice-water bath, filtered through 0.45 μm syringe filters (Spartan, Whatman). K⁺ concentrations used in this work were determined by an ion chromatograph (Aquion, Thermo Fisher Scientific, Waltham, MA, USA) equipped with a Dionex CS12A column (20 mM methanesulfonic acid as eluent). Instrument and operational details are the same as those described in Ye et al. (2017b).

WSOC and UV-Vis absorption: A quarter of each filter was extracted with 100 mL ultrapure water similar as for ionic species. The water-soluble OC (WSOC) concentrations were quantified by a TOC-VCPH analyzer (Shimadzu, Japan) using a thermo-catalytic oxidation approach. Detailed procedures are described in Ge et al. (2014). The ultraviolet–visible (UV-Vis) light absorption spectra of the water extracts were measured using a UV-Vis spectrophotometer (UV-3600, Shimadzu, Japan) as described in Zhang et al. (2013).

WSOM: The offline SP-AMS analysis details were similar to those reported previously (e.g., Ye et al., 2017a; Ye et al., 2017c). Briefly, the water extracts were nebulized with argon using a constant output atomizer (TSI Model 3076). The generated aerosols were dehumidified by a silica gel diffusion dryer, and subsequently analyzed by the SP-AMS. Purified water was aerosolized before every sample measurement to cleanse the system, and extracts of blank filters were treated in the same way as a system blank. Note the offline AMS technique was mainly used to obtain the ion-specified mass spectra of water-soluble organic matter (WSOM) (e.g., Chen et al., 2017; Daellenbach et al., 2016; Daellenbach et al., 2017; Ge et al., 2017; Ye et al., 2017a). In this work, we only used the elemental ratios determined by the SP-AMS measurements. Examples of the high resolution mass spectra (HRMS) of WSOM were presented in Fig. S2. Detailed mass spectral analyses and source apportionment of WSOM will be presented in our future work.

2.3. Data analyses

2.3.1. Light absorption coefficients

The UV–Vis light absorption data were fitted into a power law function (Hecobian et al., 2010) over the range of 300–600 nm according to:

$$\text{Abs}_\lambda = k \cdot \lambda^{-\text{Å}} \quad (1)$$

Where Abs_λ is the light absorbance at wavelength λ , k is a scaling constant, and Å is the absorption Ångström exponent (AAE) which describes the spectral dependence of light absorption from chromophores in solution.

The light absorption data is converted to an absorption coefficient at a wavelength λ (Abs_λ , M m^{-1}) by equation (2) (Hecobian et al., 2010):

$$\text{Abs}_\lambda = (A_\lambda - A_{700}) \cdot \lambda \frac{V_l}{V_a \cdot L} \ln(10) \quad (2)$$

Where A_{700} (mean value of 695–705 nm) is a reference to account for baseline drift, V_l is the volume of water that filter was extracted into, V_a is the volume of sampled air, and L is the optical path length (1 cm) of the quartz cuvette in the UV–Vis spectrometer.

The mass absorption efficiency (MAE, $\text{m}^2 \text{g}^{-1} \text{C}$) at 365 nm was then calculated by equation (3):

$$\text{MAE}_{365} = \frac{\text{Abs}_{365}}{C_{\text{WSOC}}} \quad (3)$$

Where C_{WSOC} is the WSOC concentration. We used WSOC concentrations here for consistency and comparison with previous results. In fact, as we are able to calculate the WSOM concentrations (Section 2.3.2), we can determine MAE_{365} using $\text{Abs}_{365}/C_{\text{WSOM}}$. Scatter plot of the two sets of MAE_{365} was shown in Fig. S3. They correlated very well (r of 0.96) but differed with a factor of ~ 2 as the average OM/OC ratio was ~ 2 (Section 2.3.2).

2.3.2. Elemental and OM/OC ratios of WSOM

The SP-AMS data were analyzed using the Igor-based ToF-AMS Analysis Toolkit (Squirrel v.1.57A and Pika v1.16A, available at: <http://cires.colorado.edu/jimenez-group/ToFAMSResources/ToFSoftware/>). The CO^+ signals were from fragmentation of organic species without influences from N_2^+ signals, as we used argon as carrier gas. Due to the possible influences from carbonates on organic CO_2^+ signals (Bozzetti et al., 2017; Xu et al., 2013), we set it equal to CO^+ . Signals of H_2O^+ , HO^+ and O^+ were then scaled to CO_2^+ according to Aiken et al. (2008): $\text{H}_2\text{O}^+ = 0.225 \times \text{CO}_2^+$, $\text{HO}^+ = 0.05625 \times \text{CO}_2^+$, and $\text{O}^+ = 0.009 \times \text{CO}_2^+$.

The oxygen-to-carbon (O/C) and hydrogen-to-carbon (H/C) ratios were calculated according to Canagaratna et al. (2015), nitrogen-to-carbon (N/C) ratios were derived based on Aiken et al. (2008), all of which were used to calculate the organic matter-to-organic carbon (OM/OC) ratios. The WSOM concentrations were then calculated by using the WSOC concentrations determined by the TOC analyzer (Section 2.2) and the OM/OC ratios ($\text{OM/OC}_{\text{WSOM}}$), as shown in equation (4):

$$\text{WSOM} = \text{WSOC} \cdot (\text{OM/OC})_{\text{WSOM}} \quad (4)$$

The annual average OM/OC ratio was 2.02 ± 0.1 (average $\pm 1\sigma$) (1.79–2.24), consistent with the values for WSOM reported earlier (Xu et al., 2017; Ye et al., 2017c).

2.3.3. Primary and secondary OC estimations

The EC-tracer method (Turpin and Huntzicker, 1995) was used to infer the primary OC (POC) and secondary OC (SOC), as follows:

$$\text{POC} = \text{EC} \cdot (\text{OC/EC})_{\text{pri}} \quad (5)$$

$$\text{SOC} = \text{OC} - \text{POC} \quad (6)$$

Where $(\text{OC/EC})_{\text{pri}}$ refers to the OC/EC ratio for primary OA, and the minimum measured value (1.63) among all samples was used here. It should be noted that such treatment may introduce uncertainties as the primary OA (such as biomass burning and coal combustion emissions) may have large OC/EC ratios, and the ratios also vary among different sources. However, as EC is exclusively from primary sources, the POC scaled from EC also come from primary sources; the accuracy of POC/SOC estimates is difficult to quantify, a reasonable estimate is $< 20\%$ for our study based on Wu and Yu (2016), considering the measurement uncertainties of $< 12\%$ for OC and EC (Ye et al., 2017c), an average SOC/OC of 0.65, and a sampling size of 272.

In addition, the concentrations of water-insoluble organic carbon (WIOC) can be calculated by equation (7):

$$\text{WIOC} = \text{OC} - \text{WSOC} \quad (7)$$

2.3.4. Air mass trajectories

The calculations were carried out with ZeFir, an Igor-based tool (Petit et al., 2017). The 36-h back trajectories (at 500 m height) were calculated by the HYbrid Single-Particle Lagrangian Integrated Trajectory (HYSPPLIT, version 4.8) model (Stein et al., 2016) developed by the National Oceanic and Atmospheric Administration Air Resources Laboratory.

2.3.5. Potential source contribution analyses

The potential source contribution function (PSCF) analysis was performed to explore the air mass origins and to identify potential source areas. The methodology is described elsewhere (Polissar et al., 1999). Briefly, the PSCF is calculated as:

$$\text{PSCF}_{ij} = \frac{m_{ij}}{n_{ij}} \quad (8)$$

Where n_{ij} is the total number of trajectory endpoints in the ij^{th} cell, and m_{ij} is the number of trajectory endpoints in the ij^{th} cell associated with values above the threshold value. The PSCF analysis was also carried out with the ZeFir toolkit with a resolution of $0.2^\circ \times 0.2^\circ$ for each grid cell. The 75th percentile was chosen as the threshold value to calculate m_{ij} . In order to reduce the influences of small n_{ij} on the PSCF values, a weighing function has been implemented (Petit et al., 2017):

$$w_{ij} = \begin{cases} 1.00 & \text{for } n_{ij} \geq 0.85 \max(\log(n_{ij} + 1)) \\ 0.725 & \text{for } 0.6 \max(\log(n_{ij} + 1)) < \log(n + 1) \\ & \leq 0.85 \max(\log(n_{ij} + 1)) \\ 0.475 & \text{for } 0.35 \max(\log(n_{ij} + 1)) < \log(n + 1) \\ & \leq 0.6 \max(\log(n_{ij} + 1)) \\ 0.175 & \text{for } \log(n + 1) \leq 0.35 \max(\log(n_{ij} + 1)) \end{cases} \quad (9)$$

3. Results and discussion

3.1. Wavelength dependence of light absorption

The samples were classified into spring (March–May, $n = 85$), summer (June–August, $n = 45$), fall (September–November, $n = 64$) and winter (December–February, $n = 78$). Fig. 1a presents the average light absorption spectra of the water-soluble species during four seasons and the full year within the wavelength (λ) range of 300–600 nm. Overall, the average light absorption of winter samples was significantly higher than those of spring, summer and fall, and leading to a relatively high annual absorption spectrum. This is corresponding to the high concentrations of light-absorbing species in winter samples (details in Section 3.2). The absorption intensities for all samples increased sharply towards shorter wavelengths. Such shapes are consistent with previous findings of BrC (e.g., Chen et al., 2016; Hecobian et al., 2010; Liu et al., 2013), indicating that the WSOM (or a fraction of WSOM)

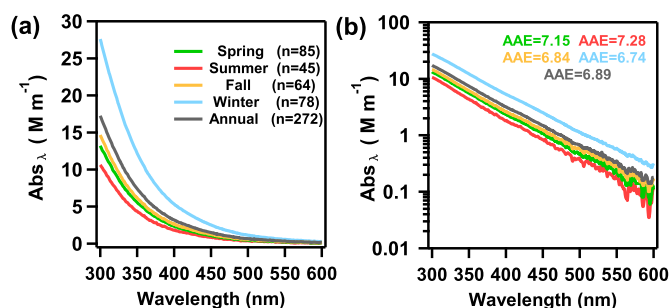


Fig. 1. Seasonal and annual averaged light absorption spectra of water-soluble aerosols: (a) linear scale and (b) log scale. The fitted Absorption Ångstrom Exponents (AAE) are shown in (b).

obtained in this study was BrC.

We further calculated the AAE values through the linear regression of $\log(\text{Abs})$ vs. $\log(\lambda)$ (the natural logarithmic form of equation (1)) in the wavelength range of 300–600 nm. The AAE values and relevant optical properties of BC and BrC can differ substantially among different situations. Several studies report that the AAE of fresh BC particles is ~ 1 (e.g., Bond, 2001; Kirchstetter et al., 2004), while the BC particles with thicker coating can have a higher AAE (as large as 1.6) even the coating species do not absorb light (Gyawali et al., 2009). Gyawali et al. (2009) also illustrates that vehicular-related and biomass burning aerosols have different optical characteristics. Much higher AAE values ranging from ~ 3 to ~ 12 are reported for water extracts of ambient aerosols collected from urban and rural sites (Cheng et al., 2016; Du et al., 2014; Kim et al., 2016; Kirillova et al., 2014; Yan et al., 2015; Zhu et al., 2017). The laboratory chamber generated particles from various wood smoldering can also have large AAE values between ~ 7 and ~ 16 (Chen and Bond, 2010). It is also worth to mention that AAE is also pH-dependent (Mo et al., 2017; Phillips et al., 2017).

In this work, the average AAE values during four seasons were 7.15, 7.28, 6.84 and 6.74, respectively (Fig. 1b). The annual average AAE value was 6.89. Different from the absorption spectra shown in Fig. 1a, the AAE value during winter was the lowest while the mean AAE of summer samples was the largest, suggesting remarkably different chemical compositions and/or sources of BrC during four seasons. Overall, the level of AAE values observed here is comparable with some previous results determined for the water-soluble $\text{PM}_{2.5}$ species extracted by using the similar extraction protocols, such as in Tibetan Plateau (6.2 and 6.9) (Zhang et al., 2017c; Zhu et al., 2017), Beijing, China (7.2–7.5) (Cheng et al., 2011), and Los Angeles basin (7.6) (Zhang et al., 2013), etc. But the AAE values also appear to be higher than those in some high-altitude Himalayas areas (3.9–5.6) (Kirillova et al., 2016), Seoul, Korea (5.84 in winter) (Kim et al., 2016). These studies demonstrate that the BrC might be related to primary biomass burning emissions and/or photochemical SOA formed from anthropogenic gaseous precursors, which are implicate for the BrC source analyses in Nanjing as well.

3.2. Seasonal variations and sources

We calculated the light absorption at 365 nm (Abs_{365} , in M m^{-1}) as a proxy to represent the light absorption of water-soluble BrC, as Abs_{365} can avoid interferences from non-organic species (such as inorganic nitrate) (Hecobian et al., 2010). The time series of Abs_{365} , MAE_{365} , RH, temperature, wind direction (colored by wind speed), and the concentrations of $\text{PM}_{2.5}$, WSOC, OC, EC and K^+ , over the full year are displayed in Fig. 2. Correspondingly, the seasonal and annual averaged values of the aerosol species, Abs_{365} and MAE_{365} are further shown in Fig. 3a. The annual average $\text{PM}_{2.5}$, OC, WSOC, EC, K^+ , Abs_{365} and MAE_{365} values were $114.5 \mu\text{g m}^{-3}$, $15.2 \mu\text{g m}^{-3}$, $7.2 \mu\text{g m}^{-3}$, $3.2 \mu\text{g m}^{-3}$, $0.7 \mu\text{g m}^{-3}$, 5.7 M m^{-1} and $0.76 \text{ m}^2 \text{ g}^{-1} \text{ C}$, respectively. In

particular, the annual MAE_{365} value is much lower than the results determined by a multi-wavelength Aethalometer (Model AE-31) in Xianghe, China (2.2 at 370 nm) (Yang et al., 2009) and Nanjing (11.4 in winter and 8.6 in summer) (Wang et al., 2018), methanol-extracted BrC in Beijing (1.45) (Cheng et al., 2016), in Los Angeles basin (2.27) (Zhang et al., 2013). But the value is also comparable with some previous values determined by online PILS-LWCC-TOC system (0.71) (Zhang et al., 2013), and those in Southeastern United States (0.64 in 8 urban sites and 0.58 in 6 rural sites) (Hecobian et al., 2010) and Central Indo Gangetic Plain (1.16) (Satish et al., 2017), etc.

The annual WSOC/OC ratio was 0.46 ± 0.1 , highest in summer (0.59 ± 0.12), followed by fall (0.49 ± 0.09), winter (0.47 ± 0.08) and spring (0.43 ± 0.12). These ratios are well within the range of WSOC/OC ratios reported earlier (Ye et al., 2017b; Zhang et al., 2018). The SOC/POC ratios were 2.11 ± 1.28 , 1.83 ± 1.19 , 2.28 ± 1.28 and 3.17 ± 1.66 in spring, summer, fall and winter, respectively. The Abs_{365} value was highest during winter ($9.44 \pm 4.70 \text{ M m}^{-1}$) and lowest during summer ($3.31 \pm 2.36 \text{ M m}^{-1}$), while the spring and fall samples had similar values of 4.32 ± 2.28 and $4.70 \pm 2.35 \text{ M m}^{-1}$, respectively. The seasonal order of Abs_{365} values was in line with their corresponding $\text{PM}_{2.5}$ /OC/WSOC concentrations, indicating the close relationships between the BrC light-absorbing ability with levels of aerosol pollution. The seasonal variability also reflected the differences of concentrations of BrC species, sources and water solubility of the light-absorbing chromophores. A similar seasonal trend of Abs_{365} is also reported in Seoul, Korea (Kim et al., 2016), but its value (0.87 – 7.31 M m^{-1}) is lower than those determined here. The Abs_{365} seasonal behavior (lowest Abs_{365} in summer and highest in winter) is also similar with those observed in other areas of China. For examples, the Abs_{365} values in Beijing, China (Du et al., 2014) are 4.6 M m^{-1} in spring, 3.7 M m^{-1} in summer, 9.1 M m^{-1} in fall and 10.1 M m^{-1} in winter; in another study, the Abs_{365} values over the southeastern Tibetan Plateau (Zhu et al., 2017) are 0.85 M m^{-1} in spring, 0.38 M m^{-1} in summer, 0.55 M m^{-1} in fall and 1.04 M m^{-1} in winter. Moreover, the MAE_{365} of the four seasons were $0.69 \text{ m}^2 \text{ g}^{-1} \text{ C}$, $0.51 \text{ m}^2 \text{ g}^{-1} \text{ C}$, $0.70 \text{ m}^2 \text{ g}^{-1} \text{ C}$ and $1.04 \text{ m}^2 \text{ g}^{-1} \text{ C}$ during spring, summer, fall and winter, respectively, which was also in the same order as that of Abs_{365} (Fig. 3a). This result highlights that for the same amount of BrC, those during winter appear to have a stronger light-absorbing ability.

Fig. 3b shows the correlation coefficients (r) of Abs_{365} versus $\text{PM}_{2.5}$, OC, WSOC, EC and K^+ for different seasons and the whole year. Generally, the correlations with WSOC were strong across four seasons (r of 0.80–0.93), and on a yearly basis, the correlation coefficient was 0.85 (Fig. 4a). Together, these results suggest that a significant fraction of WSOC is BrC chromophores and the similar sources for WSOC and water-soluble BrC throughout the year. The correlations between Abs_{365} and OC were also tight (r of 0.82–0.93) as the temporal variations of OC varied closely with WSOC in this study (r of 0.91, Fig. 4b). The correlation of Abs_{365} versus EC was weak, ranging from 0.33 to 0.51 for the four seasons (r of 0.36 for all samples). Similarly, the correlation coefficient between Abs_{365} and POC was also 0.36 (Fig. 4c) as the POC concentrations were directly scaled from EC using equation (5) in this study. On the contrary, the correlation between Abs_{365} with SOC was apparently much tighter (r of 0.86, Fig. 4e). These results demonstrate that the water-soluble BrC is abundant of secondarily formed species rather than the primary species. Correspondingly, it is expected that the SOC was strongly associated with WSOC (r of 0.89, Fig. 4f), while the POC was more likely composed of WIOC (r of 0.61, Fig. 4d). The weak correlation of water-soluble BrC Abs_{365} with POC was likely due to the low-water solubility of primary organic species, while the water-soluble BrC Abs_{365} correlated moderately with WIOC (r of 0.78, Fig. S4), likely indicating similar sources for WSOC and WIOC. Nevertheless, the light absorption properties of water-insoluble aerosol species remain to be elucidated.

In addition, K^+ ion is often used as a primary biomass burning emission tracer (Chow et al., 2007). Concentrations of this ion

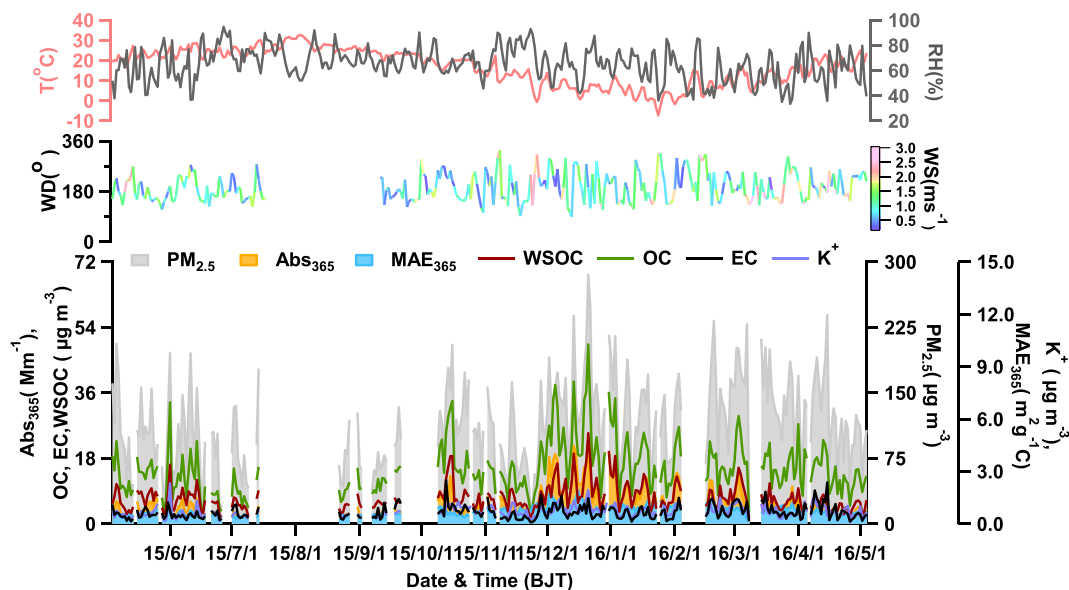


Fig. 2. Time series of (a) temperature (T) and relative humidity (RH), (b) wind direction (WD) colored by wind speed (WS), (c) PM_{2.5}, WSOC, OC, K⁺ concentrations, Abs₃₆₅ and MAE₃₆₅ during the study period (BJT, Beijing Time).

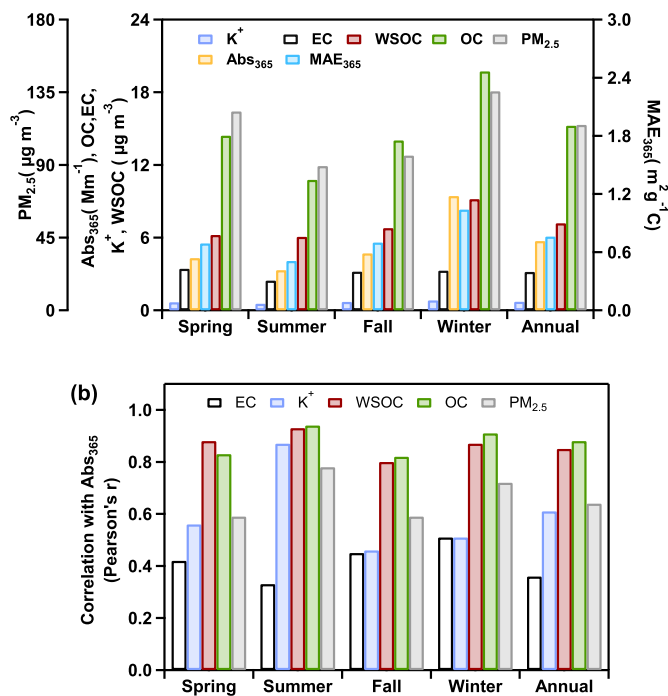


Fig. 3. (a) Seasonal and annual averaged PM_{2.5}, WSOC, OC, K⁺ concentrations, Abs₃₆₅ and MAE₃₆₅; (b) Correlation coefficients of Abs₃₆₅ versus EC, K⁺, WSOC, OC and PM_{2.5} during four seasons and the full year.

correlated much better with Abs₃₆₅ during summer (r of 0.87, Fig. 3b) than those during spring (r of 0.56), fall (r of 0.46) and winter (r of 0.51). This finding suggests that besides secondary sources, biomass burning can also contribute to the BrC evidently in summer. This is consistent with a recent study (Wang et al., 2018), which also suggests that biomass burning was an important source of BrC during summer in Nanjing. Cheng et al. (2013) also shows that K⁺ as a biomass burning tracer is reliable during summer.

As is well known, levoglucosan (C₆H₁₀O₅) is another common biomass burning tracer compound (Simoneit, 2002; Simoneit et al., 1999). Correspondingly, C₂H₄O₂⁺ and C₃H₅O₂⁺ ions are electron impact ionization fragments of levoglucosan and they are often used as biomass

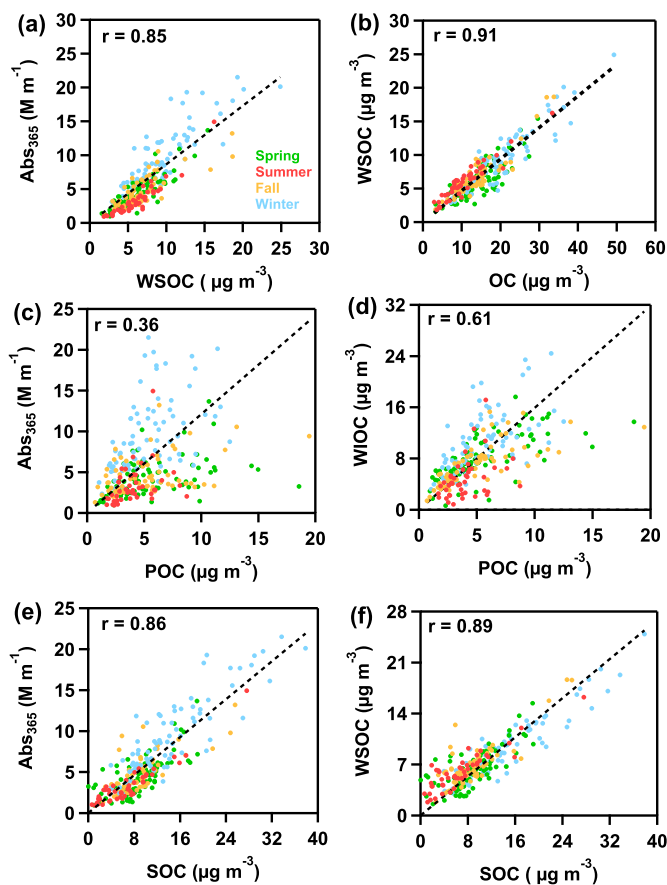


Fig. 4. Scatter plots of (a) BrC Abs₃₆₅ versus water soluble organic carbon (WSOC), (b) water-soluble organic carbon (WSOC) versus organic carbon (OC); (c) BrC Abs₃₆₅ versus primary organic carbon (POC), (d) water-insoluble organic carbon (WIOC) versus primary organic carbon (POC), (e) BrC Abs₃₆₅ versus secondary organic carbon (SOC), and (f) water-soluble organic carbon (WSOC) versus secondary organic carbon (SOC) (data are classified into four seasons).

burning OA marker ions in the AMS spectral analyses (Alfarra et al., 2007; Ge et al., 2012). Therefore, we investigated the correlations

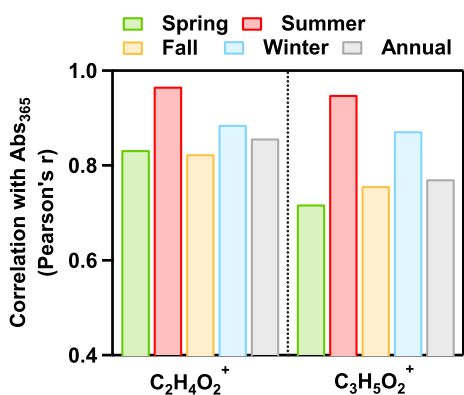


Fig. 5. Correlation coefficients of Abs_{365} versus $C_2H_4O_2^+$ and $C_3H_5O_2^+$ for the four seasons and full year.

between BrC Abs_{365} with these two AMS ions. Their concentrations were calculated based on their corresponding mass fractional contributions in the WSOM AMS spectra and the WSOM mass concentrations were derived from equation (4). As shown in Fig. 5, the BrC Abs_{365} overall showed good correlations with both $C_2H_4O_2^+$ (r of 0.83–0.97) and $C_3H_5O_2^+$ (r of 0.73–0.95). Somewhat different from the correlations with K^+ , this result indicates the possible influences of biomass burning on the BrC light absorption throughout the year. But still, summer samples correlated the best with $C_2H_4O_2^+$ (r of 0.97) and $C_3H_5O_2^+$ (r of 0.95) among four seasons, again suggesting a more obvious influence during summer than during other seasons from biomass burning. Note the good correlations with biomass burning tracer species indicate that biomass burning can contribute to the BrC, but does not mean it is the dominant contributor.

3.3. Influences of bulk chemical properties

To further unravel the features of water-soluble BrC in Nanjing, we examined the dependence of seasonal behaviors of Abs_{365} on the bulk properties of WSOM. We first plotted the Abs_{365} as a function of the average oxidation states (OS_c , defined as $2 \times O/C - H/C$) (Kroll et al., 2011) of WSOM for different seasons in Fig. 6a–d. Although there are large uncertainties, statistically the Abs_{365} values presented an increasing trend with OS_c for spring, summer and fall samples, while there was no clear positive correlation between Abs_{365} and OS_c for winter samples. Similar features were observed for Abs_{365} versus O/C ratios too in Fig. S5. Consistently, the light absorption (Abs_{365}) tended to decrease with the increase of H/C during spring, summer and fall, but the trend was less clear-cut during winter as well (Fig. S6). These plots suggest that more BrC were produced at higher OS_c . It should be noted that, previous studies report that the optical properties of atmospheric BrC species can be altered significantly during atmospheric ageing, but the ageing processes may lead to photo-enhancement (Bones et al., 2010; Updyke et al., 2012) or photo-bleaching (Lee et al., 2014; Liu et al., 2016; Sunlin et al., 2017; Zhao et al., 2015), dependent upon the types of precursors and reaction conditions. As OS_c is a metric of the ageing extent, the unique behavior of winter samples likely reflects that the dominant ageing processes or the precursors to form BrC in winter are different from those in other seasons in Nanjing. Of course, OS_c merely represents the average properties of BrC, future molecular characterization of BrC would be essential to under the ageing processes and their impacts on BrC light absorption in details. In addition, the Abs_{365} correlated very well with SOC (Fig. 4e) while the correlation with OS_c was not so tight. This is because OS_c was for WSOA while SOC was for bulk OC, and SOC itself may not perfectly correlated with OS_c as well, due to that SOC is an assemble of species from multiple oxidation processes and precursors.

To further investigate the BrC absorption efficiencies, we plotted

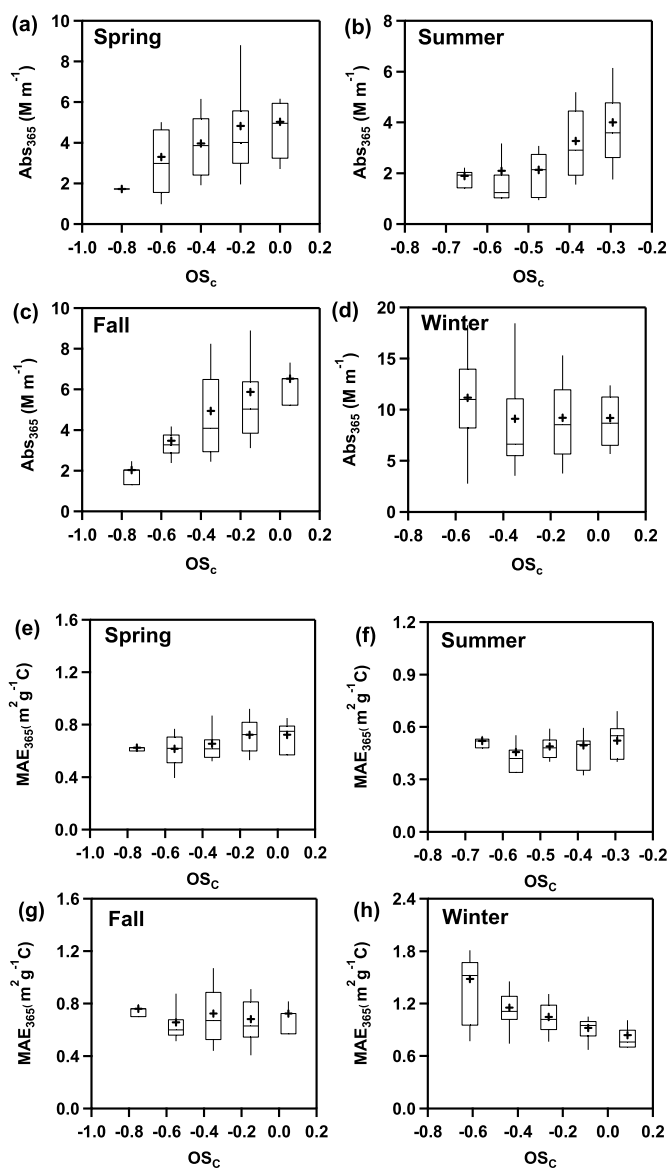


Fig. 6. Abs_{365} and MAE_{365} as a function of OS_c during spring, summer, fall and winter (Data are grouped into a few bins. The whiskers above and below indicate the 90th and 10th percentiles, the upper and lower bounds of boxes represent the 75th and 25th percentiles, and the lines and crosses inside the boxes are median and mean values).

MAE_{365} against OS_c in Fig. 6e–h. Generally, we observed no positive dependences of MAE_{365} on OS_c during spring, summer and fall, indicating that the “absorption efficiency” of WSOM did not change obviously with chemical aging during the three seasons. On the other hand, the MAE_{365} of winter WSOM presented a decreasing trend with OS_c , showing that aging may lead to photo-bleaching of WSOM in winter.

As recent studies (e.g., Budisulistiorini et al., 2017) report that nitrogen (N)- or sulfur-containing organic compounds are possible BrC chromophores. Here, we investigated Abs_{365} as well as MAE_{365} against N/C ratios during four seasons in Fig. 7 (we did not calculate Abs_{365} versus S/C ratios, as S/C ratios were very small and noisy in this work). Except a few outliers in summer and fall, generally speaking, both Abs_{365} and MAE_{365} values seemed to positively respond to the increase of N/C ratios during all time. This result manifests that N-containing organics are effective BrC light-absorbing chromophores in Nanjing. Nitroaromatic compounds were identified as important BrC compounds previously in biomass burning emissions (Cao et al., 2017; Lin et al.,

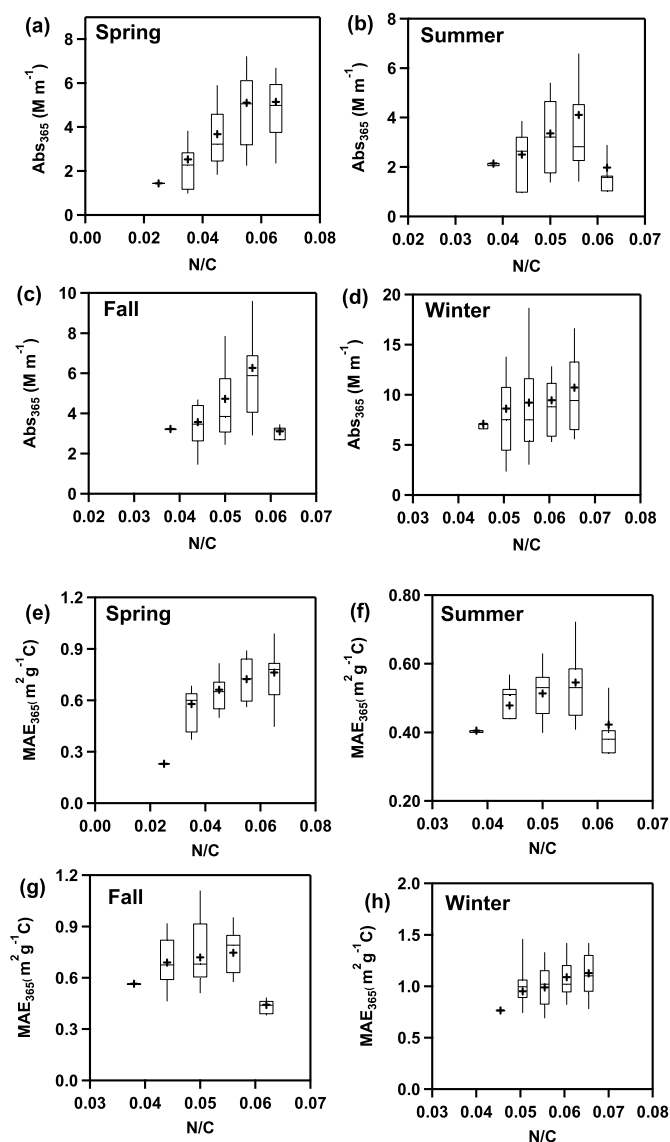


Fig. 7. Abs_{365} and MAE_{365} as a function of N/C ratios during spring, summer, fall and winter (Data are grouped into a few bins. Meanings of the boxes are the same as those described in Fig. 6).

2016). Note we indeed observed N-containing ion fragments with a benzene ring in the AMS spectra, suggesting the existence of nitroaromatics in our $PM_{2.5}$ samples even though in a very low level. Therefore, results in Fig. 7 likely verifies the possible contribution of biomass burning to BrC as well. Of course, a majority of the N-containing organic fragments in the AMS spectra are small m/z ions without a benzene ring, which are likely from other types of organic nitrogen species, including amines, amino acids, amides etc (Ge et al., 2011a; b). Whether or not these species are effective chromophores, their sources, formations and contributions to light absorption, are yet to be carefully investigated in the future.

3.4. Potential source areas

The potential source contributions (PSC) from different geological locations to the water-soluble BrC Abs_{365} are illustrated in Fig. 8. We also conducted the back trajectory analyses and presented the results in Figs. 9 and 10 for the four seasons. Winter air masses can be classified into four clusters while three clusters were identified for other seasons. There were significantly different source area contributions among four

seasons to the Abs_{365} .

During spring, the BrC potential source areas mainly distributed in the southwest and southeast of Nanjing, consistent with the cluster analyses of air mass back trajectories shown in Fig. 9a. The average values of Abs_{365} from Cluster 1 and Cluster 2 were much higher than that of Cluster 3 (Fig. 10a). Cluster 1 (46.3% of total trajectories) had a relatively short length, intercepting the local/regional emissions in the Yangtze River Delta (YRD) region. Cluster 2 (38.1%) originated from Hunan province and travelled across Anhui province, which could also play an important role in affecting the absorbability of BrC in Nanjing in spring. Cluster 3 (15.6%) started from Liaoning province, and passed through Bohai Sea, Shandong Peninsula and Huanghai Sea, which delivered relatively clean air, and had less influences on BrC. In addition, the PSC distributions of Abs_{365} were also similar to those of SOC (Fig. S7a) but not to POC (Fig. S8a) and K^+ (Fig. S9a), supporting that secondary source was a dominant contributor of BrC during spring.

During summer, the BrC potential source areas mainly located in southeast of Nanjing (< 100 km), confined within a relatively small region in Jiangsu and Anhui Provinces (Fig. 8b). Correspondingly, the air masses were also dominated by Cluster 1 (60%) with very short length (Fig. 9b). It should be noted that, the PSC hotspots of SOC (Fig. S7b), POC (Fig. S8b) and K^+ (Fig. S9b) also appeared in the southeast near Nanjing, indicating the important contributions from both primary (biomass burning) and secondary sources. Cluster 3 (17.8%) passed through the North China Plain (NCP) and the corresponding BrC seemed to be the most light-absorptive among the three clusters. Cluster 2 (22.2%) originated from Huanghai Sea and bring about less BrC compounds. In addition, maps of the fire spots in China during 2015 summer were presented in Figs. S10a–c. Obviously, lots of fire points were found in the regions overlapping with trajectories of Cluster 1 and Cluster 3, proving the biomass burning influences on BrC during summer. Such burning activities along with these clusters likely include crop burning during harvest seasons.

In fall, local Nanjing and Anhui Province were identified as the most potential source areas, as shown in Fig. 8c. Correspondingly, the BrC in Cluster 3 from such areas apparently had a higher light absorptivity than those in the other clusters (Fig. 10c), although it was not dominant (31.1%, less than 45.3% of cluster 2 from Huanghai Sea) (Fig. 9c). Also, the Abs_{365} PSC distributions were highly similar to SOC (Fig. S7c) rather than POC (Fig. S8c) and K^+ (Fig. S9c) indicating a more significant role of secondary source to BrC during fall.

For the case of winter, the potential source areas mainly located close to the sampling site (Fig. 8d). Correspondingly, the dominant air mass trajectory (Cluster 1, 52.56%) was also the shortest. Hotspots of SOC (Fig. S7d), POC (Fig. S8d) and K^+ (Fig. S9d) were all concentrated in a narrow region, all demonstrating that overall local emissions might be major sources of these species and BrC. Such local emissions may also include enhanced residential burning (such as cookstove emissions) during winter. However, on average, the BrC with large light absorptivity was not from Cluster 1, but from Cluster 2 (10.26%) and Cluster 4 (15.38%), which passed through NCP and southern China, respectively (Fig. 10d). This was also likely associated with BrC from biomass burning, and further inspection indeed found lots of fire events in these regions during February (Fig. S10f). While during the other two months, biomass burning unlikely played important roles but more likely contributions from secondary and aged local emissions were important.

4. Conclusions

This work investigated the light absorption properties and sources of water-soluble BrC in atmospheric fine particles collected from 4 May 2015 to 4 May 2016 in Nanjing. We also conducted chemical analyses of OC, EC, WSOC, K^+ , and SP-AMS analyses on the water-soluble organics. The light absorption and mass absorption efficiency at 365 nm were found to be both stronger during winter than during other

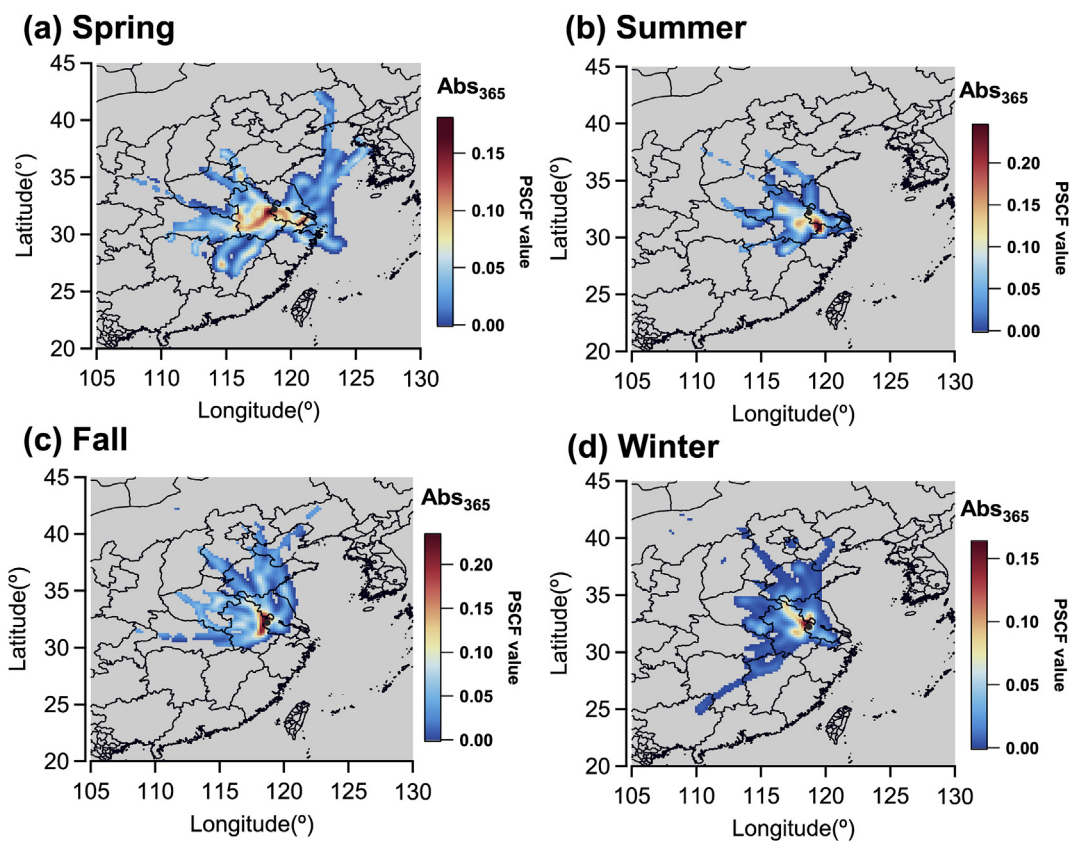


Fig. 8. The potential source contributions to BrC Abs₃₆₅ during (a) spring (b) summer (c) fall and (d) winter (colored by the PSCF values).

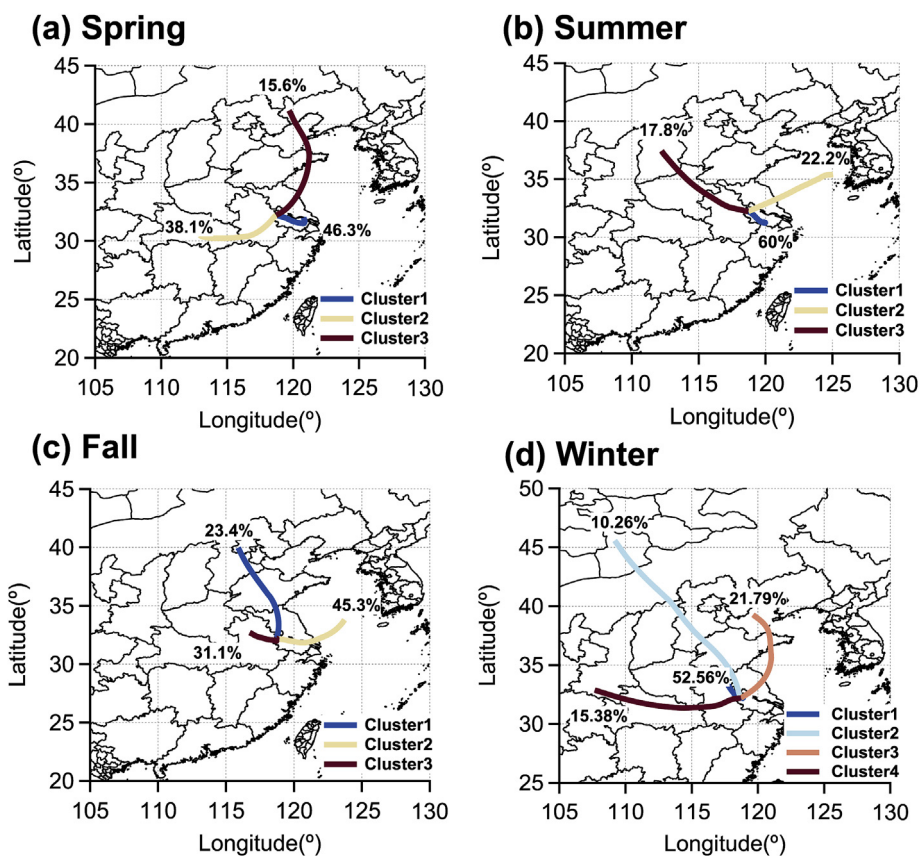


Fig. 9. Clusters of the 36-h back trajectories during (a) spring (b) summer (c) fall and (d) winter.

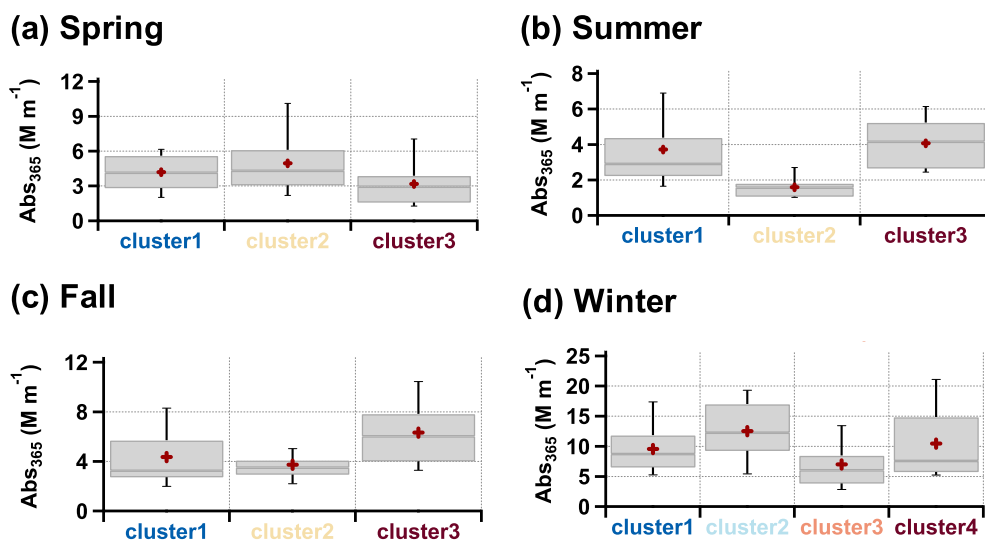


Fig. 10. The average Abs_{365} values of the different clusters during (a) spring (b) summer (c) fall and (d) winter.

seasons. The AAE values were in a range of 6.74–7.28 with an annual average of 6.89. The BrC light absorption at 365 nm (Abs_{365}) correlated very well with SOC during all seasons, indicating a significant contribution from secondary sources. We also investigated the correlation between Abs_{365} and the biomass burning marker K^+ and levoglucosan (using its AMS fragments), and found that biomass burning could contribute to BrC as well, but more evidently in summer.

The Abs_{365} generally positively responded to the increase of OS_c during spring, summer and fall, indicating more BrC at higher OS_c . While the dependences of MAE_{365} against OS_c were less clear-cut during the three seasons, MAE_{365} during winter displayed an decreasing trend against OS_c , implying chemical aging may lead to photobleaching of BrC in winter. Furthermore, overall positive correlations of both Abs_{365} and MAE_{365} with N/C ratios were found throughout the year, suggesting that nitrogen-containing organics are important BrC chromophores in Nanjing. PSCF analyses further showed the different source regions to BrC during different seasons, and in particular, pointed out that biomass burning in North China Plain or sometimes southern China could have more impacts on BrC during summer and winter (especially February in this work). Overall, our study provides valuable insights into BrC in densely populated regions. Future investigations are strongly needed, including investigation of light absorption properties of water-insoluble species, quantification of the contributions from primary and secondary sources to BrC, and the molecular characterization of possible BrC chromophores, etc.

Acknowledgements

This work was financially supported by the Natural Science Foundation of China (91544220, 21577065 and 21777073) and the Jiangsu Natural Science Foundation for distinguished young scholars (BK20150042).

Appendix A. Supplementary data

Supplementary data related to this article can be found at <http://dx.doi.org/10.1016/j.atmosenv.2018.06.002>.

References

Aiken, A.C., Decarlo, P.F., Kroll, J.H., Worsnop, D.R., Huffman, J.A., Docherty, K.S., Ulbrich, I.M., Mohr, C., Kimmel, J.R., Sueper, D., Sun, Y., Zhang, Q., Trimborn, A., Northway, M., Ziemann, P.J., Canagaratna, M.R., Onasch, T.B., Alfarra, M.R., Prevot, A.S.H., Dommen, J., Duplissy, J., Metzger, A., Baltensperger, U., Jimenez, J.L., 2008. O/C and OM/OC ratios of primary, secondary, and ambient organic aerosols with

high-resolution time-of-flight aerosol mass spectrometry. *Environ. Sci. Technol.* 42, 4478–4485.

Alfarra, M.R., Prevot, A.S.H., Szidat, S., Sandradewi, J., Weimer, S., Lanz, V.A., Schreiber, D., Mohr, M., Baltensperger, U., 2007. Identification of the mass spectral signature of organic aerosols from wood burning emissions. *Environ. Sci. Technol.* 41, 5770–5777.

Bahadur, R., Praveen, P.S., Xu, Y., Ramanathan, V., 2012. Solar absorption by elemental and brown carbon determined from spectral observations. *P. Natl. Acad. Sci. USA* 109, 17366–17371.

Birch, M.E., Cary, R.A., 1996. Elemental carbon-based method for monitoring occupational exposures to particulate diesel exhaust. *Aerosol. Sci. Technol.* 25, 221–241.

Bond, T.C., 2001. Spectral dependence of visible light absorption by carbonaceous particles emitted from coal combustion. *Geophys. Res. Lett.* 28, 4075–4078.

Bond, T.C., Covert, D.S., Kramlich, J.C., Larson, T.V., Charlson, R.J., 2002. Primary particle emissions from residential coal burning: optical properties and size distributions. *J. Geophys. Res. Atmos.* 107, 8347.

Bond, T.C., Doherty, S.J., Fahey, D.W., Forster, P.M., Bernsten, T., DeAngelo, B.J., Flanner, M.G., Ghan, S., Kärcher, B., Koch, D., Kinne, S., Kondo, Y., Quinn, P.K., Sarofim, M.C., Schultz, M.G., Schulz, M., Venkataraman, C., Zhang, H., Zhang, S., Bellouin, N., Guttikunda, S.K., Hopke, P.K., Jacobson, M.Z., Kaiser, J.W., Klimont, Z., Lohmann, U., Schwarz, J.P., Shindell, D., Storelvmo, T., Warren, S.G., Zender, C.S., 2013. Bounding the role of black carbon in the climate system: a scientific assessment. *J. Geophys. Res. Atmos.* 118, 5380–5552.

Bones, D.L., Henriksen, D.K., Mang, S.A., Gonsior, M., Bateman, A.P., Nguyen, T.B., Cooper, W.J., Nizkorodov, S.A., 2010. Appearance of strong absorbers and fluorophores in limonene-O-3 secondary organic aerosol due to NH_4^+ -mediated chemical aging over long time scales. *J. Geophys. Res. Atmos.* 115, D05203.

Bozzetti, C., Sosedova, Y., Xiao, M., Daellenbach, K.R., Uleviccius, V., Dudoitis, V., Mordas, G., Byčenkienė, S., Plauškaitė, K., Vlachou, A., Golly, B., Chazeau, B., Besombes, J.-L., Baltensperger, U., Jaffrezo, J.-L., Slowik, J.G., El Haddad, I., Prévôt, A.S.H., 2017. Argon offline-AMS source apportionment of organic aerosol over yearly cycles for an urban, rural, and marine site in northern Europe. *Atmos. Chem. Phys.* 17, 117–141.

Budisulistiorini, S.H., Riva, M., Williams, M., Chen, J., Itoh, M., Surratt, J.D., Kuwata, M., 2017. Light-absorbing brown carbon aerosol constituents from combustion of Indonesian peat and biomass. *Environ. Sci. Technol.* 51, 4415–4423.

Canagaratna, M.R., Jimenez, J.L., Kroll, J.H., Chen, Q., Kessler, S.H., Massoli, P., Hildebrandt Ruiz, L., Fortner, E., Williams, L.R., Wilson, K.R., Surratt, J.D., Donahue, N.M., Jayne, J.T., Worsnop, D.R., 2015. Elemental ratio measurements of organic compounds using aerosol mass spectrometry: characterization, improved calibration, and implications. *Atmos. Chem. Phys.* 15, 253–272.

Cao, F., Zhang, S., Kawamura, K., Liu, X., Yang, C., Xu, Z., Fan, M., Zhang, W., Bao, M., Chang, Y., Song, W., Liu, S., Lee, X., Li, J., Zhang, G., Zhang, Y., 2017. Chemical characteristics of dicarboxylic acids and related organic compounds in PM_{2.5} during biomass-burning and non-biomass-burning seasons at a rural site of Northeast China. *Environ. Pollut.* 231, 654–662.

Cappa, C.D., Onasch, T.B., Massoli, P., Worsnop, D.R., Bates, T.S., Cross, E.S., Davidovits, P., Hakala, J., Hayden, K.L., Jobson, B.T., Kolesar, K.R., Lack, D.A., Lerner, B.M., Li, S.-M., Mellon, D., Nuaaman, I., Olfert, J.S., Petäjä, T., Quinn, P.K., Song, C., Subramanian, R., Williams, E.J., Zaveri, R.A., 2012. Radiative absorption enhancements due to the mixing state of atmospheric black carbon. *Science* 337, 1078–1081.

Carlsaw, K.S., Boucher, O., Spracklen, D.V., Mann, G.W., Rae, J.G.L., Woodward, S., Kulmala, M., 2010. A review of natural aerosol interactions and feedbacks within the Earth system. *Atmos. Chem. Phys.* 10, 1701–1737.

Chakrabarty, R.K., Moosmüller, H., Chen, L.W.A., Lewis, K., Arnott, W.P., Mazzoleni, C., Dubey, M.K., Wold, C.E., Hao, W.M., Kreidenweis, S.M., 2010. Brown carbon in tar balls from smoldering biomass combustion. *Atmos. Chem. Phys.* 10, 6363–6370.

Chen, Q., Ikemori, F., Mochida, M., 2016. Light absorption and excitation-emission

- fluorescence of urban organic aerosol components and their relationship to chemical structure. *Environ. Sci. Technol.* 50, 10859–10868.
- Chen, Q., Ikemori, F., Nakamura, Y., Vodicka, P., Kawamura, K., Mochida, M., 2017. Structural and light-absorption characteristics of complex water-insoluble organic mixtures in urban submicron aerosols. *Environ. Sci. Technol.* 51, 8293–8303.
- Chen, Y., Bond, T.C., 2010. Light absorption by organic carbon from wood combustion. *Atmos. Chem. Phys.* 10, 1773–1787.
- Cheng, Y., Engling, G., He, K.B., Duan, F.K., Ma, Y.L., Du, Z.Y., Liu, J.M., Zheng, M., Weber, R.J., 2013. Biomass burning contribution to Beijing aerosol. *Atmos. Chem. Phys.* 13, 7765–7781.
- Cheng, Y., He, K., Du, Z., Engling, G., Liu, J., Ma, Y., Zheng, M., Weber, R.J., 2016. The characteristics of brown carbon aerosol during winter in Beijing. *Atmos. Environ.* 127, 355–364.
- Cheng, Y., He, K., Zheng, M., Duan, F., Du, Z., Ma, Y., Tan, J., Yang, F., Liu, J., Zhang, X., Weber, R., Bergin, M., Russell, A., 2011. Mass absorption efficiency of elemental carbon and water-soluble organic carbon in Beijing, China. *Atmos. Chem. Phys.* 11, 11497–11510.
- Chow, J.C., Watson, J.G., Lowenthal, D.H., Chen, L.W.A., Zielinska, B., Mazzoleni, L.R., Magliano, K.L., 2007. Evaluation of organic markers for chemical mass balance source apportionment at the Fresno SuperSite. *Atmos. Chem. Phys.* 7, 1741–1754.
- Daellenbach, K.R., Bozzetti, C., Křepelová, A., Canonaco, F., Wolf, R., Zotter, P., Fermo, P., Crippa, M., Slowik, J.G., Sosedova, Y., Zhang, Y., Huang, R.J., Poulain, L., Szidat, S., Baltensperger, U., El Haddad, I., Prévôt, A.S.H., 2016. Characterization and source apportionment of organic aerosol using offline aerosol mass spectrometry. *Atmos. Meas. Tech.* 9, 23–39.
- Daellenbach, K.R., Stefenelli, G., Bozzetti, C., Vlachou, A., Fermo, P., Gonzalez, R., Piazzalunga, A., Colombi, C., Canonaco, F., Hueglin, C., 2017. Long-term chemical analysis and organic aerosol source apportionment at 9 sites in Central Europe: source identification and uncertainty assessment. *Atmos. Chem. Phys.* 17, 13265–13282.
- Desyaterik, Y., Sun, Y., Shen, X., Lee, T., Wang, X., Wang, T., Collett, J.L., 2013. Speciation of “brown” carbon in cloud water impacted by agricultural biomass burning in eastern China. *J. Geophys. Res. Atmos.* 118, 7389–7399.
- Du, Z., He, K., Cheng, Y., Duan, F., Ma, Y., Liu, J., Zhang, X., Zheng, M., Weber, R., 2014. A yearlong study of water-soluble organic carbon in Beijing II: light absorption properties. *Atmos. Environ.* 89, 235–241.
- Feng, Y., Ramanathan, V., Kotamarthi, V.R., 2013. Brown carbon: a significant atmospheric absorber of solar radiation? *Atmos. Chem. Phys.* 13, 8607–8621.
- Ge, X., Li, L., Chen, Y., Chen, H., Wu, D., Wang, J., Xie, X., Ge, S., Ye, Z., Xu, J., Chen, M., 2017. Aerosol characteristics and sources in Yangzhou, China resolved by offline aerosol mass spectrometry and other techniques. *Environ. Pollut.* 225, 74–85.
- Ge, X., Setyan, A., Sun, Y., Zhang, Q., 2012. Primary and secondary organic aerosols in Fresno, California during wintertime: results from high resolution aerosol mass spectrometry. *J. Geophys. Res. Atmos.* 117, D19301.
- Ge, X., Shaw, S.L., Zhang, Q., 2014. Toward understanding amines and their degradation products from postcombustion CO₂ capture processes with aerosol mass spectrometry. *Environ. Sci. Technol.* 48, 5066–5075.
- Ge, X., Wexler, A.S., Clegg, S.L., 2011a. Atmospheric amines - Part I. A review. *Atmos. Environ.* 45, 524–546.
- Ge, X., Wexler, A.S., Clegg, S.L., 2011b. Atmospheric amines - Part II. Thermodynamic properties and gas/particle partitioning. *Atmos. Environ.* 45, 561–577.
- Gyawali, M., Arnott, W.P., Lewis, K., Moosmüller, H., 2009. In situ aerosol optics in Reno, NV, USA during and after the summer 2008 California wildfires and the influence of absorbing and non-absorbing organic coatings on spectral light absorption. *Atmos. Chem. Phys.* 9, 8007–8015.
- Hecobian, A., Zhang, X., Zheng, M., Frank, N., Edgerton, E.S., Weber, R.J., 2010. Water-soluble organic aerosol material and the light-absorption characteristics of aqueous extracts measured over the Southeastern United States. *Atmos. Chem. Phys.* 10, 5965–5977.
- Hems, R.F., Abbatt, J.P.D., 2018. Aqueous phase photo-oxidation of brown carbon n-trophenols: reaction kinetics, mechanism, and evolution of light absorption. *ACS Earth Space Chem.* 2, 225–234.
- Kim, H., Kim, J.Y., Jin, H.C., Lee, J.Y., Lee, S.P., 2016. Seasonal variations in the light-absorbing properties of water-soluble and insoluble organic aerosols in Seoul, Korea. *Atmos. Environ.* 129, 234–242.
- Kirchstetter, T.W., Novakov, T., Hobbs, P.V., 2004. Evidence that the spectral dependence of light absorption by aerosols is affected by organic carbon. *J. Geophys. Res. Atmos.* 109, D21208.
- Kirillova, E.N., Andersson, A., Tiwari, S., Srivastava, A.K., Bisht, D.S., Gustafsson, Ö., 2014. Water-soluble organic carbon aerosols during a full New Delhi winter: isotope-based source apportionment and optical properties. *J. Geophys. Res. Atmos.* 119, 3476–3485.
- Kirillova, E.N., Marinoni, A., Bonasoni, P., Vuillemoz, E., Facchini, M.C., Fuzzi, S., Decesari, S., 2016. Light absorption properties of brown carbon in the high Himalayas. *J. Geophys. Res. Atmos.* 121, 9621–9639.
- Kroll, J.H., Donahue, N.M., Jimenez, J.L., Kessler, S.H., Canagaratna, M.R., Wilson, K.R., Altieri, K.E., Mazzoleni, L.R., Wozniak, A.S., Bluhm, H., 2011. Carbon oxidation state as a metric for describing the chemistry of atmospheric organic aerosol. *Nat. Chem.* 3, 133.
- Lack, D.A., Langridge, J.M., Bahreini, R., Cappa, C.D., Middlebrook, A.M., Schwarz, J.P., 2012a. Brown carbon and internal mixing in biomass burning particles. *P. Natl. Acad. Sci. USA* 109, 14802–14807.
- Lack, D.A., Lovejoy, E.R., Baynard, T., Pettersson, A., Ravishankara, A.R., 2006. Aerosol absorption measurement using photoacoustic spectroscopy: sensitivity, calibration, and uncertainty developments. *Atmos. Sci. Technol.* 40, 697–708.
- Lack, D.A., Richardson, M.S., Law, D., Langridge, J.M., Cappa, C.D., McLaughlin, R.J., Murphy, D.M., 2012b. Aircraft instrument for comprehensive characterization of aerosol optical properties, Part 2: black and brown carbon absorption and absorption enhancement measured with photo acoustic spectroscopy. *Aerosol. Sci. Technol.* 46, 555–568.
- Laskin, A., Laskin, J., Nizkorodov, S.A., 2015. Chemistry of atmospheric brown carbon. *Chem. Rev.* 115, 4335–4382.
- Lee, H.J., Aiona, P.K., Laskin, A., Laskin, J., Nizkorodov, S.A., 2014. Effect of solar radiation on the optical properties and molecular composition of laboratory proxies of atmospheric brown carbon. *Environ. Sci. Technol.* 48, 10217–10226.
- Lin, P., Aiona, P.K., Li, Y., Shiraiwa, M., Laskin, J., Nizkorodov, S.A., Laskin, A., 2016. Molecular characterization of brown carbon in biomass burning aerosol particles. *Environ. Sci. Technol.* 50, 11815–11824.
- Lin, P., Liu, J., Shilling, J.E., Kathmann, S.M., Laskin, J., Laskin, A., 2015. Molecular characterization of brown carbon (BrC) chromophores in secondary organic aerosol generated from photo-oxidation of toluene. *Phys. Chem. Chem. Phys. : Phys. Chem. Chem. Phys.* 17, 23312–23325.
- Liu, J., Bergin, M., Guo, H., King, L., Kotra, N., Edgerton, E., Weber, R.J., 2013. Size-resolved measurements of brown carbon in water and methanol extracts and estimates of their contribution to ambient fine-particle light absorption. *Atmos. Chem. Phys.* 13, 12389–12404.
- Liu, J., Lin, P., Laskin, A., Laskin, J., Kathmann, S.M., Wise, M., Caylor, R., Imholt, F., Selimovic, V., Shilling, J.E., 2016. Optical properties and aging of light-absorbing secondary organic aerosol. *Atmos. Chem. Phys.* 16, 12815–12827.
- Liu, J., Scheuer, E., Dibb, J., Diskin, G.S., Ziemba, L.D., Thornhill, K.L., Anderson, B.E., Wisthaler, A., Mikoviny, T., Devi, J.J., 2015. Brown carbon aerosol in the North American continental troposphere: sources, abundance, and radiative forcing. *Atmos. Chem. Phys.* 15, 5959–6007.
- Mo, Y., Li, J., Liu, J., Zhong, G., Cheng, Z., Tian, C., Chen, Y., Zhang, G., 2017. The influence of solvent and pH on determination of the light absorption properties of water-soluble brown carbon. *Atmos. Environ.* 161, 90–98.
- Nakayama, T., Ikeda, Y., Sawada, Y., Setoguchi, Y., Ogawa, S., Kawana, K., Mochida, M., Ikemori, F., Matsumoto, K., Matsumi, Y., 2015. Properties of light-absorbing aerosols in the Nagoya urban area, Japan, in August 2011 and January 2012: contributions of brown carbon and lensing effect. *J. Geophys. Res. Atmos.* 119, 7127–7127, 739.
- Nguyen, T.B., Lee, P.B., Updyke, K.M., Bones, D.L., Laskin, J., Laskin, A., Nizkorodov, S.A., 2012. Formation of nitrogen- and sulfur-containing light-absorbing compounds accelerated by evaporation of water from secondary organic aerosols. *J. Geophys. Res. Atmos.* 117.
- Petit, J.E., Favez, O., Albinet, A., Canonaco, F., 2017. A user-friendly tool for comprehensive evaluation of the geographical origins of atmospheric pollution: wind and trajectory analyses. *Environ. Model. Software* 88, 183–187.
- Phillips, S.M., Bellcross, A.D., Smith, G.D., 2017. Light absorption by brown carbon in the southeastern United States is pH-dependent. *Environ. Sci. Technol.* 51, 6782–6790.
- Pokhrel, R.P., Beamesderfer, E.R., Wagner, N.L., Langridge, J.M., Lack, D.A., Jayarathne, T., Stone, E.A., Stockwell, C.E., Yokelson, R.J., Murphy, S.M., 2017. Relative importance of black carbon, brown carbon, and absorption enhancement from clear coatings in biomass burning emissions. *Atmos. Chem. Phys.* 17, 5063–5078.
- Pokhrel, R.P., Wagner, N.L., Langridge, J.M., Lack, D.A., Jayarathne, T., Stone, E.A., Stockwell, C.E., Yokelson, R.J., Murphy, S.M., 2016. Parameterization of single-scattering albedo (SSA) and absorption Ångström exponent (AAE) with EC/OC for aerosol emissions from biomass burning. *Atmos. Chem. Phys.* 16, 9549–9561.
- Polissar, A.V., Hopke, P.K., Paatero, P., Kaufmann, Y.J., Hall, D.K., Bodhaine, B.A., Dutton, E.G., Harris, J.M., 1999. The aerosol at Barrow, Alaska: long-term trends and source locations. *Atmos. Environ.* 33, 2441–2458.
- Saleh, R., Hennigan, C.J., McMeeking, G.R., Chuang, W.K., Robinson, E.S., Coe, H., Donahue, N.M., Robinson, A.L., 2013. Absorptivity of brown carbon in fresh and photo-chemically aged biomass-burning emissions. *Atmos. Chem. Phys.* 13, 7683–7693.
- Saleh, R., Robinson, E.S., Tkacik, D.S., Ahern, A.T., Liu, S., Aiken, A.C., Sullivan, R.C., Presto, A.A., Dubey, M.K., Yokelson, R.J., Donahue, N.M., Robinson, A.L., 2014. Brownness of organics in aerosols from biomass burning linked to their black carbon content. *Nat. Geosci.* 7, 647.
- Satish, R., Shamjad, P., Thamban, N., Tripathi, S., Rastogi, N., 2017. Temporal characteristics of brown carbon over the central Indo-Gangetic plain. *Environ. Sci. Technol.* 51, 6765–6772.
- Shamjad, P.M., Tripathi, S.N., Pathak, R., Hallquist, M., Arola, A., Bergin, M.H., 2015. Contribution of brown carbon to direct radiative forcing over the Indo-Gangetic plain. *Environ. Sci. Technol.* 49, 10474–10481.
- Simoneit, B.R.T., 2002. Biomass burning — a review of organic tracers for smoke from incomplete combustion. *Appl. Geochem.* 17, 129–162.
- Simoneit, B.R.T., Schauer, J.J., Nolte, C.G., Oros, D.R., Elias, V.O., Fraser, M.P., Rogge, W.F., Cass, G.R., 1999. Levoglucosan, a tracer for cellulose in biomass burning and atmospheric particles. *Atmos. Environ.* 33, 173–182.
- Stein, A.F., Draxler, R.R., Rolph, G.D., Stunder, B.J.B., Cohen, M.D., Ngan, F., 2016. NOAA's HYSPLIT atmospheric transport and dispersion modeling system. *Bull. Am. Meteorol. Soc.* 96, 150504130527006.
- Sumlin, B.J., Pandey, A., Walker, M.J., Pattison, R.S., Williams, B.J., Chakrabarty, R.K., 2017. Atmospheric photooxidation diminishes light absorption by primary brown carbon aerosol from biomass burning. *Environ. Sci. Technol. Lett.* 4, 540–545.
- Teich, M., van Pinxteren, D., Wang, M., Kecorius, S., Wang, Z., Müller, T., Močnik, G., Herrmann, H., 2017. Contributions of nitrated aromatic compounds to the light absorption of water-soluble and particulate brown carbon in different atmospheric environments in Germany and China. *Atmos. Chem. Phys.* 17, 1653–1672.
- Turpin, B.J., Huntzicker, J.J., 1995. Identification of secondary organic aerosol episodes and quantification of primary and secondary organic aerosol concentrations during SCAQS. *Atmos. Environ.* 29, 3527–3544.

- Updyke, K.M., Nguyen, T.B., Nizkorodov, S.A., 2012. Formation of brown carbon via reactions of ammonia with secondary organic aerosols from biogenic and anthropogenic precursors. *Atmos. Environ.* 63, 22–31.
- Wang, G., Chen, C., Li, J., Zhou, B., Xie, M., Hu, S., Kawamura, K., Chen, Y., 2011. Molecular composition and size distribution of sugars, sugar-alcohols and carboxylic acids in airborne particles during a severe urban haze event caused by wheat straw burning. *Atmos. Environ.* 45, 2473–2479.
- Wang, G., Kawamura, K., Xie, M., Hu, S., Cao, J., An, Z., Waston, J.G., Chow, J.C., 2009. Organic molecular compositions and size distributions of Chinese summer and autumn aerosols from Nanjing: characteristic haze event caused by wheat straw burning. *Environ. Sci. Technol.* 43, 6493–6499.
- Wang, G., Kawamura, K., Zhao, X., Li, Q., Dai, Z., Niu, H., 2007. Identification, abundance and seasonal variation of anthropogenic organic aerosols from a mega-city in China. *Atmos. Environ.* 41, 407–416.
- Wang, J., Ge, X., Chen, Y., Shen, Y., Zhang, Q., Sun, Y., Xu, J., Ge, S., Yu, H., Chen, M., 2016a. Highly time-resolved urban aerosol characteristics during springtime in Yangtze River Delta, China: insights from soot particle aerosol mass spectrometry. *Atmos. Chem. Phys.* 16, 9109–9127.
- Wang, J., Nie, W., Cheng, Y., Shen, Y., Chi, X., Wang, J., Huang, X., Xie, Y., Sun, P., Xu, Z., Qi, X., Su, H., Ding, A., 2018. Light absorption of brown carbon in eastern China based on 3-year multi-wavelength aerosol optical property observations at the SORPES station and an improved Absorption Ångström exponent segregation method. *Atmos. Chem. Phys. Discuss.* 1–31.
- Wang, J., Onasch, T.B., Ge, X., Collier, S., Zhang, Q., Sun, Y., Yu, H., Chen, M., Prévôt, A.S., Worsnop, D.R., 2016b. Observation of fullerene soot in eastern China. *Environ. Sci. Technol. Lett.* 3, 121–126.
- Wang, J., Zhang, Q., Chen, M., Collier, S., Zhou, S., Ge, X., Xu, J., Shi, J., Xie, C., Hu, J., Ge, S., Sun, Y., Coe, H., 2017. First chemical characterization of refractory black carbon aerosols and associated coatings over the Tibetan plateau (4730 m a.s.l.). *Environ. Sci. Technol.* 51, 14072–14082.
- Washenfelder, R.A., Attwood, A.R., Brock, C.A., Guo, H., Xu, L., Weber, R.J., Ng, N.L., Allen, H.M., Ayres, B.R., Baumann, K., Cohen, R.C., Draper, D.C., Duffey, K.C., Edgerton, E., Fry, J.L., Hu, W.W., Jimenez, J.L., Palm, B.B., Romer, P., Stone, E.A., Wooldridge, P.J., Brown, S.S., 2015. Biomass burning dominates brown carbon absorption in the rural southeastern United States. *Geophys. Res. Lett.* 42, 653–664.
- Wu, C., Yu, J.Z., 2016. Determination of primary combustion source organic carbon-to-elemental carbon (OC/EC) ratio using ambient OC and EC measurements: secondary OC-EC correlation minimization method. *Atmos. Chem. Phys.* 16, 5453–5465.
- Wu, D., Zhang, F., Ge, X., Yang, M., Xia, J., Liu, G., Li, F., 2017. Chemical and light extinction characteristics of atmospheric aerosols in suburban Nanjing, China. *Atmosphere* 8, 149.
- Xie, M., Chen, X., Hays, M.D., Lewandowski, M., Offenberg, J., Kleindienst, T.E., Holder, A.L., 2017. Light absorption of secondary organic aerosol: composition and contribution of nitroaromatic compounds. *Environ. Sci. Technol.* 51, 11607–11616.
- Xu, J., Zhang, Q., Li, X., Ge, X., Xiao, C., Ren, J., Qin, D., 2013. Dissolved organic matter and inorganic ions in a central Himalayan glacier—insights into chemical composition and atmospheric sources. *Environ. Sci. Technol.* 47, 6181–6188.
- Xu, L., Guo, H., Weber, R.J., Ng, N.L., 2017. Chemical characterization of water-soluble organic aerosol in contrasting rural and urban environments in the southeastern United States. *Environ. Sci. Technol.* 51, 78–88.
- Yan, C., Zheng, M., Bosch, C., Andersson, A., Desyaterik, Y., Sullivan, A.P., Collett, J.L., Zhao, B., Wang, S., He, K., Gustafsson, O., 2017. Important fossil source contribution to brown carbon in Beijing during winter. *Sci. Rep.* 7, 43182.
- Yan, C., Zheng, M., Sullivan, A.P., Bosch, C., Desyaterik, Y., Andersson, A., Li, X., Guo, X., Zhou, T., Gustafsson, Ö., Collett, J.L., 2015. Chemical characteristics and light-absorbing property of water-soluble organic carbon in Beijing: biomass burning contributions. *Atmos. Environ.* 121, 4–12.
- Yang, M., Howell, S.G., Zhuang, J., Huebert, B.J., 2009. Attribution of aerosol light absorption to black carbon, brown carbon, and dust in China – interpretations of atmospheric measurements during EAST-AIRE. *Atmos. Chem. Phys.* 9, 2035–2050.
- Ye, Z., Li, Q., Liu, J., Luo, S., Zhou, Q., Bi, C., Ma, S., Chen, Y., Chen, H., Li, L., Ge, X., 2017a. Investigation of submicron aerosol characteristics in Changzhou, China: composition, source, and comparison with co-collected PM_{2.5}. *Chemosphere* 183, 176–185.
- Ye, Z., Li, Q., Ma, S., Zhou, Q., Gu, Y., Su, Y., Chen, Y., Chen, H., Wang, J., Ge, X., 2017b. Summertime day-night differences of PM_{2.5} components (inorganic ions, OC, EC, WSOC, WSON, HULIS, and PAHs) in Changzhou, China. *Atmosphere* 8, 189.
- Ye, Z., Liu, J., Gu, A., Feng, F., Liu, Y., Bi, C., Xu, J., Li, L., Chen, H., Chen, Y., Dai, L., Zhou, Q., Ge, X., 2017c. Chemical characterization of fine particulate matter in Changzhou, China, and source apportionment with offline aerosol mass spectrometry. *Atmos. Chem. Phys.* 17, 2573–2592.
- Zhang, X., Lin, Y., Surratt, J.D., Weber, R.J., 2013. Sources, composition and absorption Ångström exponent of light-absorbing organic components in aerosol extracts from the Los Angeles Basin. *Environ. Sci. Technol.* 47, 3685–3693.
- Zhang, Y.-L., El-Haddad, I., Huang, R.-J., Ho, K.-F., Cao, J.-J., Han, Y., Zotter, P., Bozzetti, C., Daellenbach, K.R., Slowik, J.G., Salazar, G., Prévôt, A.S.H., Szidat, S., 2018. Large contribution of fossil fuel derived secondary organic carbon to water soluble organic aerosols in winter haze in China. *Atmos. Chem. Phys.* 18, 4005–4017.
- Zhang, Y., Forrister, H., Liu, J., Dibb, J., Anderson, B., Schwarz, J.P., Perring, A.E., Jimenez, J.L., Campuzano-Jost, P., Wang, Y., Nenes, A., Weber, R.J., 2017a. Top-of-atmosphere radiative forcing affected by brown carbon in the upper troposphere. *Nat. Geosci.* 10, 486–489.
- Zhang, Y., Tang, L., Sun, Y., Favez, O., Canonaco, F., Albinet, A., Couvidat, F., Liu, D., Jayne, J.T., Wang, Z., 2017b. Limited formation of isoprene epoxydiols-derived secondary organic aerosol under NO_x-rich environments in Eastern China. *Geophys. Res. Lett.* 44, 2035–2043.
- Zhang, Y., Tang, L., Yu, H., Wang, Z., Sun, Y., Qin, W., Chen, W., Chen, C., Ding, A., Wu, J., 2015. Chemical composition, sources and evolution processes of aerosol at an urban site in Yangtze River Delta, China during wintertime. *Atmos. Environ.* 123, 339–349.
- Zhang, Y., Xu, J., Shi, J., Xie, C., Ge, X., Wang, J., Kang, S., Zhang, Q., 2017c. Light absorption by water-soluble organic carbon in atmospheric fine particles in the central Tibetan Plateau. *Environ. Sci. Pollut. Res.* 24, 21386–21397.
- Zhao, R., Lee, A.K.Y., Huang, L., Li, X., Yang, F., Abbatt, J.P.D., 2015. Photochemical processing of aqueous atmospheric brown carbon. *Atmos. Chem. Phys.* 15, 6087–6100.
- Zhong, M., Jang, M., 2011. Light absorption coefficient measurement of SOA using a UV-Visible spectrometer connected with an integrating sphere. *Atmos. Environ.* 45, 4263–4271.
- Zhu, C., Cao, J., Huang, R., Shen, Z., Wang, Q., Zhang, N., 2017. Light absorption properties of brown carbon over the southeastern Tibetan Plateau. *Sci. Total Environ.* 625, 246–251.